ISSN: 2438-442X

Transactions on Machine Design

DLINE JOURNALS

TMD 2024; 12 (1)
https://doi.org/10.6025/tmd/2024/12/1/1-19

Improvement of the test Method for the Thermal Integrity of Cast-in-place Pile Tip: Optimizing The Layout of Temperature Measuring Points

Zhiguo Ma[1], Chenjin Shi[1], Yuan Hou[1], Chao Xue[1], Minghao Sun[2] and Yong Zeng[2]

[1]PowerChina Roadbridge Group CO. LTD, Beijing, China

[2]School of Civil Engineering, Southwest Jiaotong University, Chengdu, China.

{zengy@swjtu.edu.cn}

Received: 18 August 2023
Revised: 15 November 2023
Accepted: 27 November 2023

ABSTRACT

Due to the nature of underground structures, detecting defects in pile foundations is very difficult. Many methods for detecting such defects are currently in use, with various advantages and disadvantages. A new defect detection method has been proposed—thermal integrity detection. When an abnormal concrete temperature occurs, this abnormality is attributed to a defect within the concrete. When the temperature is elevated, it is attributed to bulging; when the temperature is depressed, it is attributed to necking, mud entrapment, or hollowing. Using finite element analysis can make the identification of defects quantifiable, but the study of concrete defects in pile foundations becomes complicated due to undesirable choice of temperature measurement point locations, reducing the efficiency and accuracy of finite element inverse analysis. Based on previous research, the location of temperature measurement points is optimized in this work. First, the effect of the change of reinforcement position on the concrete temperature field is studied, and it is confirmed that the change of reinforcement position affects only the location of the measurement points, not the concrete temperature field itself. Then measurement points on the concrete surface are selected for finite element inverse analysis of the pile temperature field and the results are compared with measurements in the field. The new measurement points can avoid irrelevant factors in the finite element inverse analysis of the pile foundation temperature field. The complexity of the finite element inverse analysis is greatly reduced, and the accuracy of defect location and size identification is improved.

Keywords: *Thermal Integrity Testing, Pile Foundation Defect Detection, Temperature Measurement Points, Finite Element, Heat Transfer*

1. Introduction

With the rapid development of China's economy, more and more pile foundations will be used in bridges and high-rise buildings. As the span of bridges and the height of buildings increase, the use of larger-diameter and longer pile foundations will become the norm. At present, most pile foundations use bored piles, whose integrity and quality are critical to the safety of the structures.

Quality inspection of pile foundations is therefore particularly important. However, the nature of the underground hidden structure itself (e.g., limited accessibility, low visibility, and considerable depth) makes the inspection of pile foundations exceptionally difficult [1-2].

The traditional methods for detecting defects of grouted piles include low-strain, high-strain, borehole-coring, and acoustic-projection methods. These traditional defect detection methods have problems that are difficult to overcome in practice. First, high (low) strain detection is easily affected by the surrounding environment, which is not sensitive to small defects and cannot obtain information on the horizontal location of defects. Second, high (low) strain detection for grouted piles makes it difficult to calculate the elastic modulus, leading to inaccurate calculation of pile length and defect depth. The borehole-coring method is limited by a hole, which is sometimes not accurate enough to determine local defects or horizontal cracks in the pile foundation. It may also cause some damage to the pile foundation. When using the acoustic transmission method of detection, the pile to be tested needs to be accompanied by a pre-buried acoustic tube, increasing the cost of the pile foundation. This method can only detect defects in the contact tube, causing a certain detection blind area. This makes it difficult to detect small horizontal cracks. Also, this method cannot be applied to uncured concrete piles.

In recent years, the use of thermal integrity to determine pile foundation defects has emerged. The principle of this method is as follows: If there are no defects in the concrete in the same soil layer, the temperature at different sections of the concrete will be the same. If there is an abnormality in the temperature at a particular cross-section, it indicates the presence of defects and attributes an increase in temperature to bulging and a decrease in temperature to necking, mud trapping, or cavitation [3]. Two main ways to use thermal integrity to determine pile defects are the distributed temperature sensor (DTS) detection method and the thermal integrity profiler (TIP) detection method. The DTS method targets mainly piles that have been cast and formed. Its principle is to insert a distributed fiber-optic sensor into the formed pile foundation and then heat the fiber to form a temperature field inside the concrete. The distributed fiber-optic sensor also comes with a temperature measurement function, and the specific location of pile foundation defects can be determined by the data read by the sensor [4-6]. In addition, some researchers have combined finite element simulation with the DTS detection method in order to investigate the thermal integrity of the formed pile foundation [7].

However, the DTS detection method is applied less often during pile-foundation construction, when it is more common to use the TIP detection method. Unlike the DTS detection method, the TIP detection method involves attaching the temperature-measuring instrument to the reinforcement cage before the concrete is placed. The temperature of the concrete can then be measured while the concrete is being placed. Additional heating of the measuring instrument is not needed due to the heat of hydration of the concrete [8-11]. The TIP detection method can detect defects at an earlier stage of concrete hydration than the DTS detection method, and avoid remediation after the pile foundation is formed. Thus, the TIP detection method is now primarily used in pile construction. On this basis, Sun et al. [10] combined the finite element method with the inverse analysis of the pile foundation defects and improved the existing TIP detection method.

However, there is an obvious problem with the existing TIP detection method. As the temperature measurement device is tied directly to the reinforcement cage, the position of the cage may be altered during the lowering process. And the concrete's own temperature field will change after the cage is moved. In addition, the position of the measurement point will also change. So, the displacement of the cage must be considered when using the TIP detection method to find concrete defects. The direction of the cage displacement is random, which also makes it more difficult to find the defects. In addition, the displacement of the cage needs to be considered when using finite elements for inverse analysis of defects, which leads to a rapid increase in the number of finite element inverse analyses. Also, the results of the inverse analyses can differ greatly from the actual values. It is therefore necessary to further optimize the existing TIP inspection method, and then improve its application.

In this work, the existing TIP inspection method is improved based on an actual highway bridge pile foundation project. A sandbag was used to simulate the mud trapping defect, and

the location and size of the defect were initially determined by the field measurement results. A numerical model was used to investigate the influence of the location of the reinforcement cage on the concrete temperature field, so as to have a preliminary determination of the location of the temperature measurement point. Next, the selected measurement point was used to carry out finite element inverse analysis of the defect, and the results of the inverse analysis were compared with the actual measurement results. The results illustrate the superiority of the improved TIP inspection method.

2. Experimental Site and Instruments

The experiment was located at the construction site of a particular highway bridge pile foundation. The stratigraphic condition of the site is shown in Table 1. The depth of the groundwater level is 12.6m, but it was pumped completely dry after drilling. A bored pile with a design length of 70m was used in the experiment. The diameter of the upper 25m of the pile is 2.8m and the diameter of its reinforcement cage is 2.67m. The diameter of the lower 45m of the pile is 2.2m and the diameter of its reinforcement cage is 2.07m. At depths of 10, 20, 25, 30, 40, 45, 50, and 60m, four temperature measurement points were evenly arranged along the circumference of the pile. In addition, four temperature sensors were evenly arranged along the wall of each section at depths of 40 and 45m. The geometric structure of the pile foundation and the distribution of the temperature sensors are shown in Figure 1, Figure 2 and Figure 3 show the temperature measuring device and the field experimental device respectively.

The temperature sensors were fixed by means of a rebar cage, while the outer temperature sensors at 40 and 45m were fixed at designated locations on the shaft wall by a special set of devices. During the lowering of the reinforcement cage, the cable connected to the temperature sensor was run upwards. Then, when the cage was lowered into place, the cable was connected to the data-acquisition instrument, and data acquisition started on May 27, 2022. Concrete pouring started at 4:50 a.m. on May 28, 2022 and was completed at 10:16 a.m. on the same day the data were collected by the collection instrument every hour for 100 hours after the completion of the pour and were then collected every 8 hours for a total of 360 hours.

In this experiment, there was an inclusion located at 40 m, as shown in Figure 4. The inclusions were sand bags of 0.2-m thickness filled with sandy soil, which surrounded the reinforcement cage for one week.

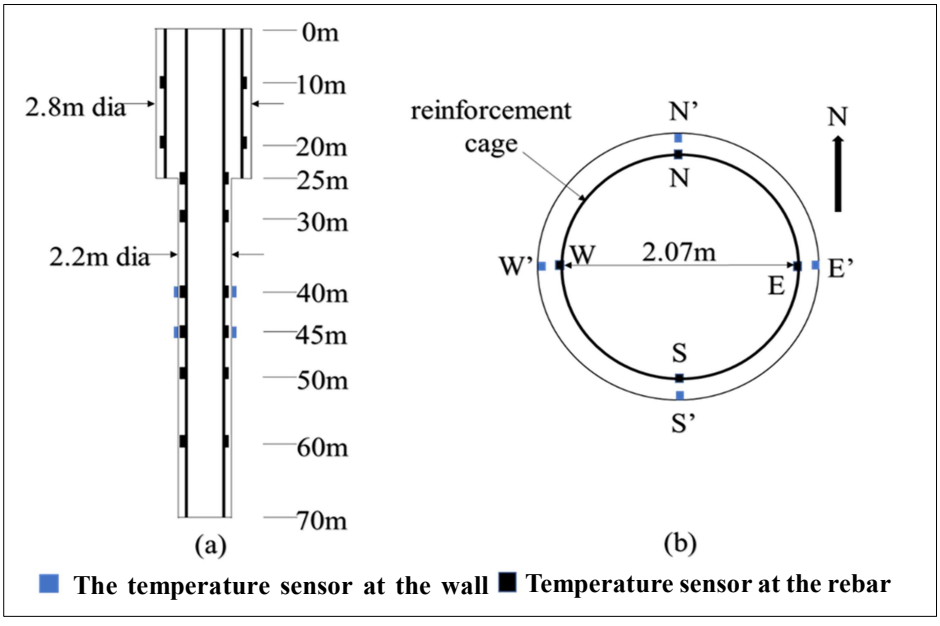

Figure 1. Pile geometry and arrangement of temperature-measurement points (a) in the direction of pile length and (b) at 40 and 45*m* sections

Figure 2. Temperature measuring equipment

Depth range (*m*)	Stratigraphic lithology
0~9.4	*Pebbles*
9.4~70	*Fully weathered conglomerate*

Table 1. Stratigraphic lithology

Figure 3. Reinforcement cage

3. Analysis of Measured Data

If the test pile is intact and free of defects, if the reinforcement cage is centrally located, and if the soil properties are consistent, the temperature measured by different temperature sensors in the same soil layer should be the same. The variation of soil thermal properties between different strata affects the rate of heat dissipation from the concrete body to the surrounding ground. Where the soil thermal conductivity is high and the heat transfer rate is rapid, the temperature of the corresponding strata is lower in the longitudinal (pile length direction) temperature profile. In addition, the infill piles used in this study were not of equal diameter and had abrupt changes in diameter at 25m, leading to a change in the axial temperature field of the pile foundations. This needs to be taken into account in the data analysis.

Given that the hydration rate of concrete varies with time, the best moments to determine the defects of concrete have been proposed in some papers [9,12,13]. First is the moment with the fastest rate of change of temperature; second is the moment with the highest temperature. In this study, the moment with the fastest rate of temperature rise was 10h after casting, and the moment with the highest temperature was 66h after casting. The heat of hydration of concrete decreased significantly at 200h after casting. Accordingly, the concrete temperatures at these three time points were chosen for analysis. The temperature variation curves along the longitudinal direction of the experimental pile base measured at three different stages are shown in Figure 5.

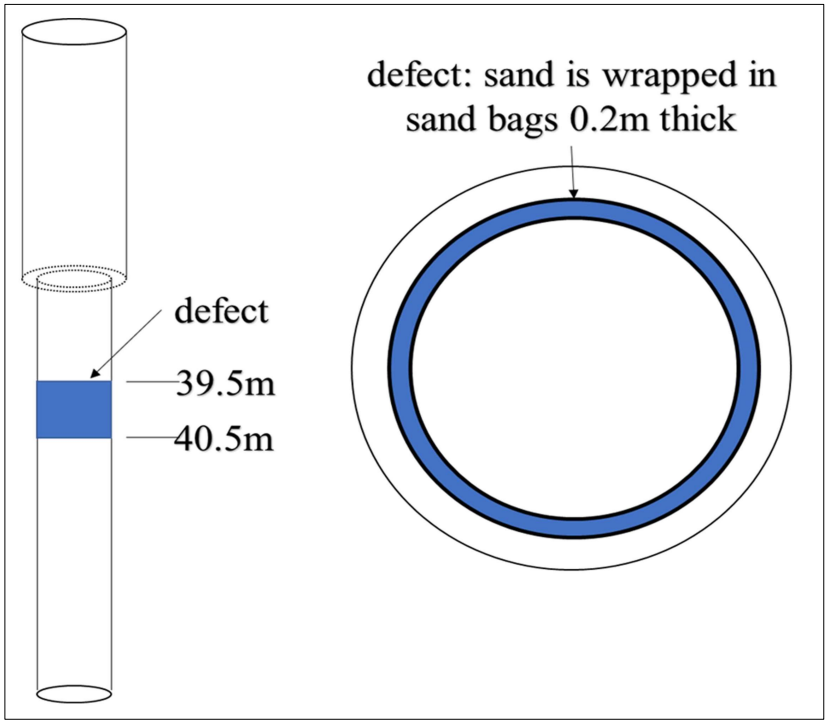

Figure 4. Engineering inclusions in field experiments

Figure 5. In this figure the letters N, E, S, and W are used to indicate measurement points at the north, east, south, and west sides, respectively, of each section at different depths. In addition to the measured data at each measurement point, the graph also includes the temperature variation curve along the longitudinal direction of the experimental pile base in the absence of defects.

It can be seen from Figure 3 that whether it is 10, 66, or 200h after the completion of pouring, the temperatures measured at the reinforcement located in the depth range of 30-45m is significantly less than the theoretical value. This indicates that there must be defects in this

range, which is within the range of the set mud trapping defects (39.5-40.5m). The temperatures measured at the four measurement points at a depth of 20m were slightly higher than the theoretical value, which indicates that the defect of bulging may exist here, but to only a slight degree. Temperatures at a depth of 25m were slightly below the theoretical value, indicating a possible defect. But it is not yet possible to determine what type (or types) of defect may have been causing the measured temperature to be below the theoretical value - necking, mud trapping, and cavities can all cause a drop in concrete temperature.

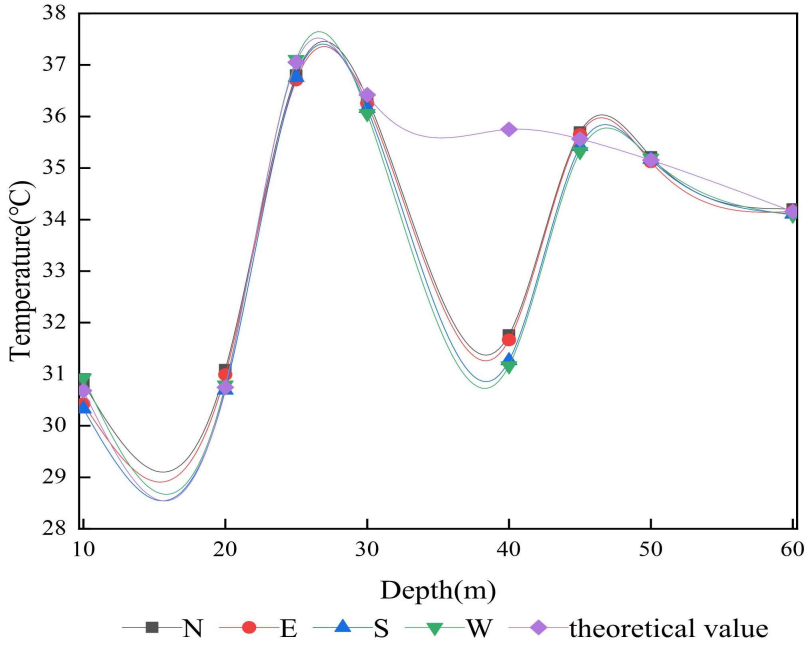

(a) 10 h after pouring completed

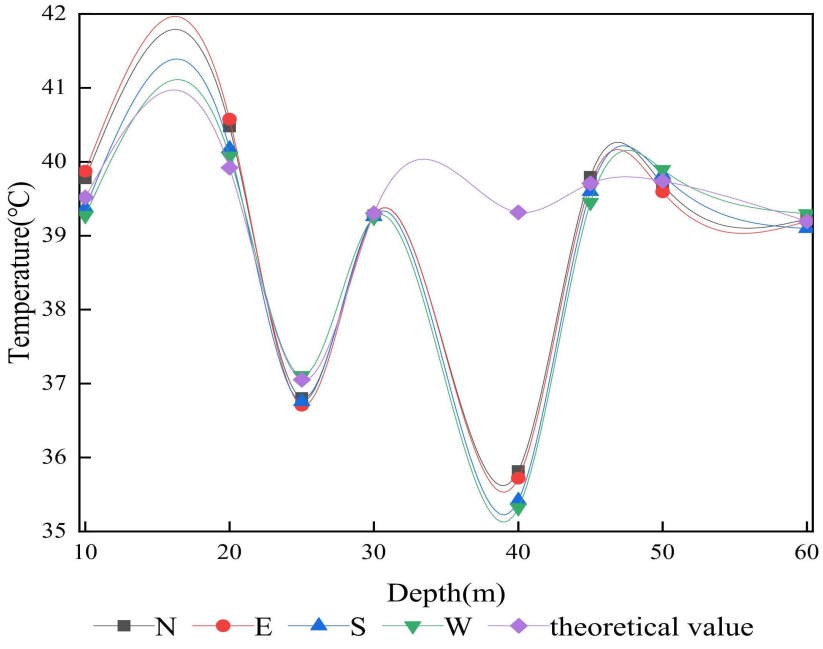

(b) 66 h after pouring completed

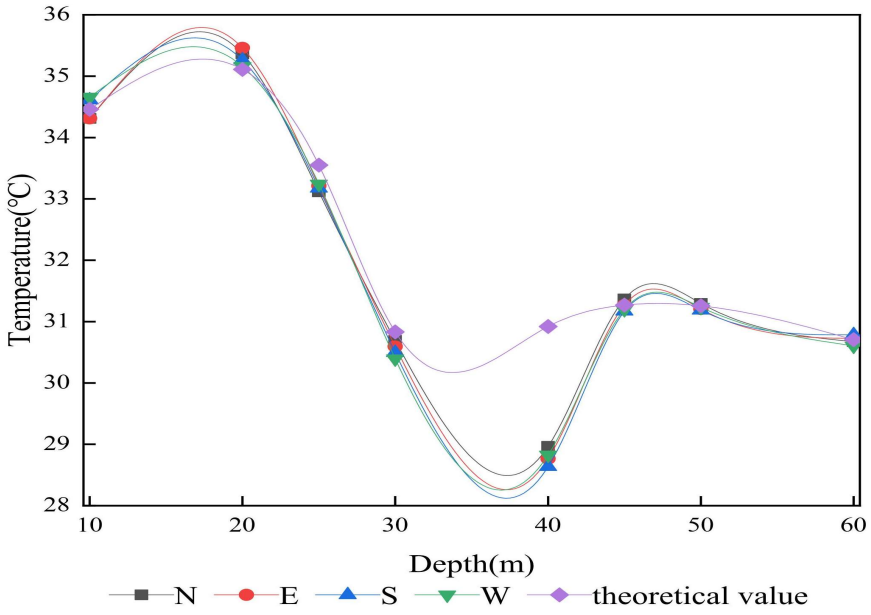

Figure 5. Longitudinal temperature variation profiles of pile concrete at different moments

Some of the measured points at 10m were slightly above and someslightly below the theoretical values. In the absence of pre-determined defects in this section, it is believed that a slight deflection of the reinforcement cage in this section may have occurred, although the presence of some defects cannot be ruled out.

The above analysis shows that the experimental results can only qualitatively determine the presence or absence of defects and their types. In order to quantitatively determine the defects, it is necessary to further establish a finite element model for pile foundation temperature field analysis, conduct a series of finite element analyses, and inverse analyze the effect of these defects on the temperature field.

4. Numerical Analysis

4.1. Finite Element Model

In this work, a finite element model was established to simulate the hydration and heat-transfer processes of concrete. The concrete temperature field can be calculated by using the heat-transfer equation and specific boundary conditions with initial conditions to solve the heat transfer equation [14].

$$\frac{\partial T}{\partial \tau} = \frac{\lambda}{c\rho}\left(\frac{\partial^2 T}{\partial x} + \frac{\partial^2 T}{\partial y} + \frac{\partial^2 T}{\partial z}\right) + \frac{\partial \theta}{\partial \tau} \quad (1)$$

where λ is the thermal conductivity of concrete (kJ•(m•h•C)-1), c is the specific heat capacity of concrete (kJ•(kg•C)-1). τ is time (h), ρ is the density of concrete (kg/m3), and è is the adiabatic temperature rise of concrete (°C).

There are four types of boundary conditions for the temperature field. In this work, the concrete at the top surface of the pile foundation is in contact with the air and the heat transfer between them satisfies the third type of boundary condition. An expression of the third type of boundary condition is

$$\lambda \frac{\partial T}{\partial x} = h(T_e - T_c) \quad (2)$$

where h is the convective heat transfer coefficient of the concrete surface(W•(m2•K)-1), Te is the ambient temperature (°C), and Tc is the concrete surface temperature (°C). The value of h is determined by [15]

$$h = 3.06v + 4.11 \tag{3}$$

where v is wind speed (m/s). According to the actual wind speed measured on site, v is taken as 2.5m/s.

The heat transfer between concrete and rock, inclusions and reinforcement, satisfies the Type 4 boundary condition. There are two forms for this type of boundary condition, which are applicable to the cases of complete and incomplete contact between the two solids. Here, we consider the case where the concrete is in complete contact with the rock and reinforcement. Expressions for the fourth type of boundary conditions are given by

$$\lambda_1 \frac{\partial T_1}{\partial n} = \lambda_2 \frac{\partial T_2}{\partial n} \tag{4}$$

$$T_1 = T_2 \tag{5}$$

The initial temperature of the rock, inclusions, and reinforcement was taken from the temperature sensor attached to the steel cage before the concrete was placed. It was 14 °C. The initial temperature of the concrete placement was 21°C.

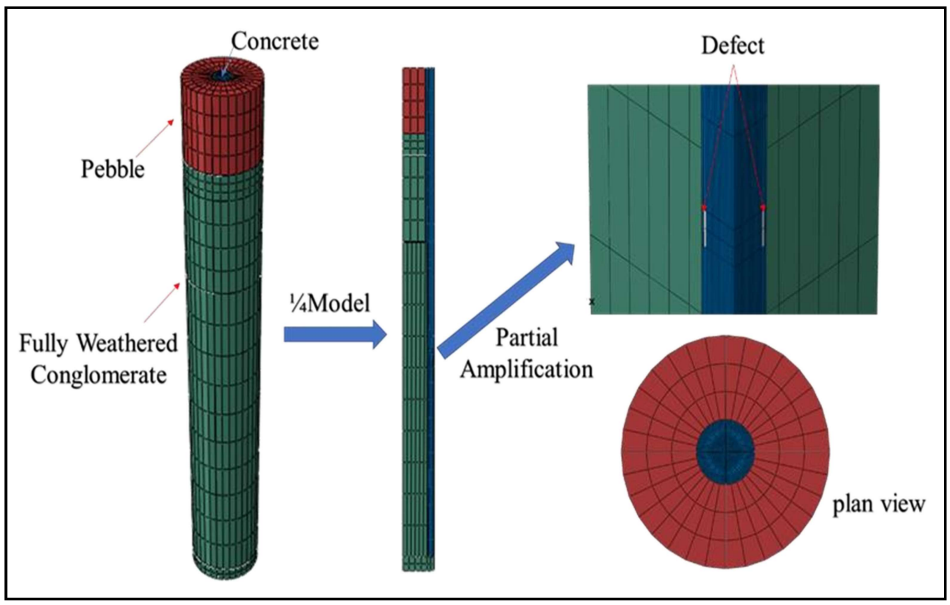

Figure 6. Finite element mesh for pile foundation detection

Using the equations described previously, a finite element model was established using ABAQUS software, as shown in Figure 4. According to an existing study [16], the maximum distance of heat of hydration transfer in the rock body along the horizontal direction within 48h after the completion of concrete placement is 3m. Therefore, the radius of the rock body analysis of the layer where the pile foundation is located was set to 6m. The length and radius of the pile concrete were established according to the values marked on the construction drawings. The number of reinforcement bars was taken as the number of bars used in the actual construction, and it was assumed that all the bars were placed at the predetermined positions without deflection.

The shape of the defect was assumed to be a cylindrical ring. In the simulation analysis, DC3D8 eight-node linear heat transfer hexahedron element was used for thecalculation of concrete, defects and rocks, and DC1D2 two-node heat transfer connection element was used for the calculation of reinforcement. Thus, 17,200 units were considered in this model.

Material Property	Fully weathered conglomerate	Concrete	Rebar	Pebble	Occluded foreign substance
Density/(*kg*/*m*3)	1700	2410	7850	2610	2700
Specific heat capacity/ [*J*•(*kg*• C)-1]	720	933	460	780	1300
Thermal conductivity / [*kJ*/(*m*•*h*•C)]	8.96	10.71	260	7.92	7.2

Table 2. Thermal parameters of related materials

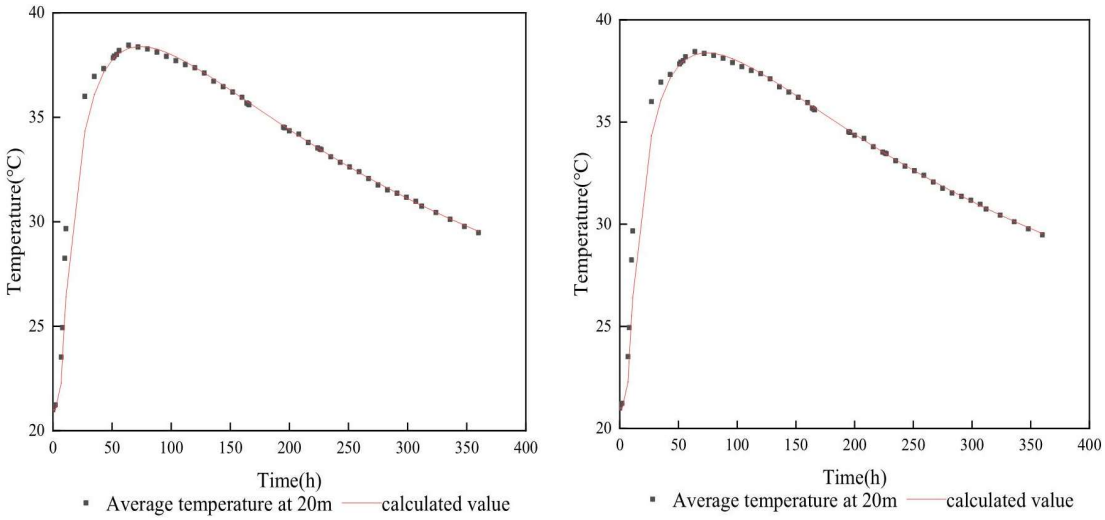

(a) 20-*m* position **(b) 60-m position**

Figure 7. Comparison of results of finite element calculations and field measurements

The specific heat capacity and thermal conductivity of concrete are usually measured by a concrete thermal performance test. However, a concrete thermal performance test was not conducted in this work due to the limited field test conditions. Thus, the calculation of specific heat capacity and thermal conductivity of concrete was carried out with reference to the estimation method proposed by Zhu Bofang[14]. The density of concrete was obtained from field measurements as 2410kg/m3. The density, specific heat capacity, and thermal conductivity of rebar, pebble, weathered conglomerate, and inclusions were obtained from field thermal performance tests. The thermal parameters of various materials are shown in Table 2.

The accuracy of the heat of hydration model of concrete directly affects the accuracy of the finite element calculation results. Many researchers have studied the heat of hydration model for concrete over the years. De-Schutter [17] established a classical hydration model based

on the results of isothermal and adiabatic cement calorimetric tests, and improved the model by another series of tests at a later stage. Zhu Bofang[14,18] established three models of the time-dependence of the heat of hydration of concrete under adiabatic conditions: exponential, double exponential, and hyperbolic. But none of the three models considered the slow induction period in the early stage of the concrete hydration reaction. Schindler and Folliard[19] proposed a hydration model based on the maturity of concrete. The equivalent age of concrete and the Arrhenius rate theory were used to represent the heat production rate. Then the model was optimized by regressing the data from many cement experiments to express explicitly some material parameters. On this basis, an S-type formula that is more consistent *with the hydration reaction rate was proposed by Sudo Xue et al. [20]. The heat of hydration model of concrete proposed by these researchers was used in this study. It has a clear and relatively simple formula.*

$$\theta(t) = \theta_0 \, me^{-\frac{n}{\tau}} \tag{6}$$

Where $\theta 0$ is the final adiabatic temperature rise of concrete (C°), m and n are constants to be determined, and $\theta(t)$ is the adiabatic temperature rise of concrete at time t (C°).

The final adiabatic temperature rise of concrete can be calculated using the equation [21]

$$\theta_0 = \frac{Q_0 W'_C}{c\rho} \tag{7}$$

where W'_C is the converted cement mass per unit volume (kg/m3). According to this equation, the final adiabatic temperature rise of concrete can be calculated to be 45.95°C.

The two parameters m and n in Equation (6) can be obtained by fitting a curve to the experimental concrete adiabatic temperature rise. They are found to be $m = 1.3$ and $n = 5$.

Using the above parameters, the average values of concrete section temperature measurements at depths of 20 and 60 m were selected for verification. They are shown in Figure 5. From this figure, it can be seen that the results calculated by using the finite element software match well the field-measured results, which supports the correctness of the finite element model.

4.2. Effect of Reinforcement Displacement on the Concrete Temperature field

In addition to the soil layer and defects, the offset of the reinforcement may also affect the measured temperature distribution. As mentioned in the Introduction, the effect of reinforcement displacement on the concrete temperature field may result from two things. First, the difference in the position of the reinforcement will have an effect on the concrete temperature field itself. Second, when the position of the reinforcement changes, the position of the temperature sensor will also change since the temperature sensor is tied to the reinforcement, the measured temperature is not the temperature at the corresponding measurement point. It is therefore necessary to analyze the effect of the position of the reinforcement on the concrete temperature field when constructing the finite element model.

The cross section of the studied bored pile is circular with a perfect symmetry. Thus, it is only necessary to translate the surrounding reinforcement by a distance in the same direction when exploring the effect of reinforcement position on the concrete temperature field. The specific translation method and range are shown in Figure 6. According to the different positions of the reinforcement bars, the temperature dependence on time at typical measurement points at 25-m depth after the concrete placement was completed is shown in Figure 7.

As can be seen from this figure, when the reinforcement bars were located at different positions, both at the point in the center of the concrete and at the point at the edge of the concrete, their temperature curves with time coincide almost exactly. And the maximum temperature difference was less than 0.1C°. Considering the accuracy of the temperature sensor, it can be assumed that the rebar position has no effect on the concrete temperature field itself. It

affects only the position of the temperature sensor tied to the reinforcement. Therefore, the position of the reinforcement can be considered as if no displacement occurred in the process of finite element modeling. But it is necessary to pay attention to the position of the reinforcement in the cross-section when dividing the mesh.

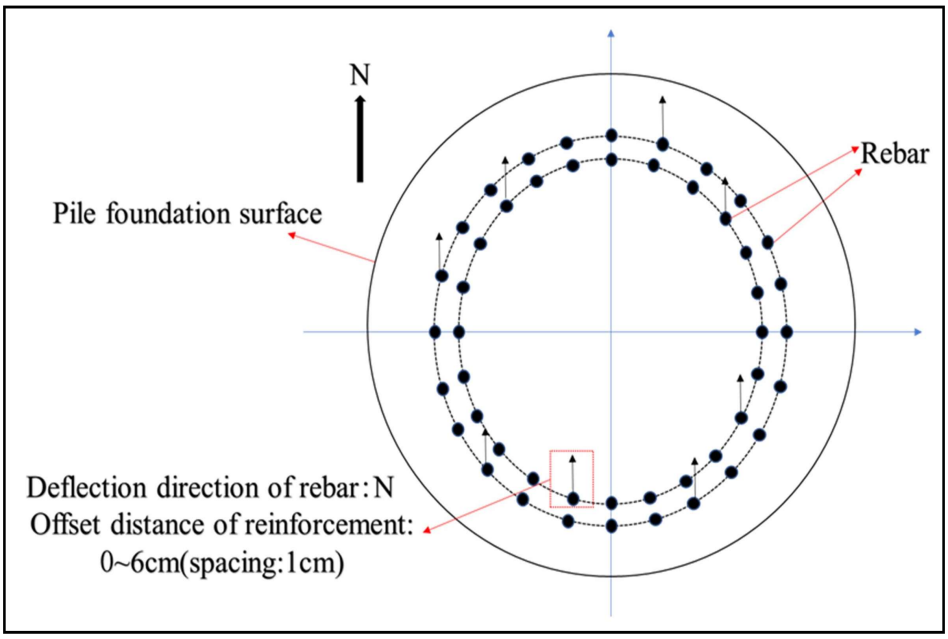

Figure 8. Schematic diagrams of rebar displacement method

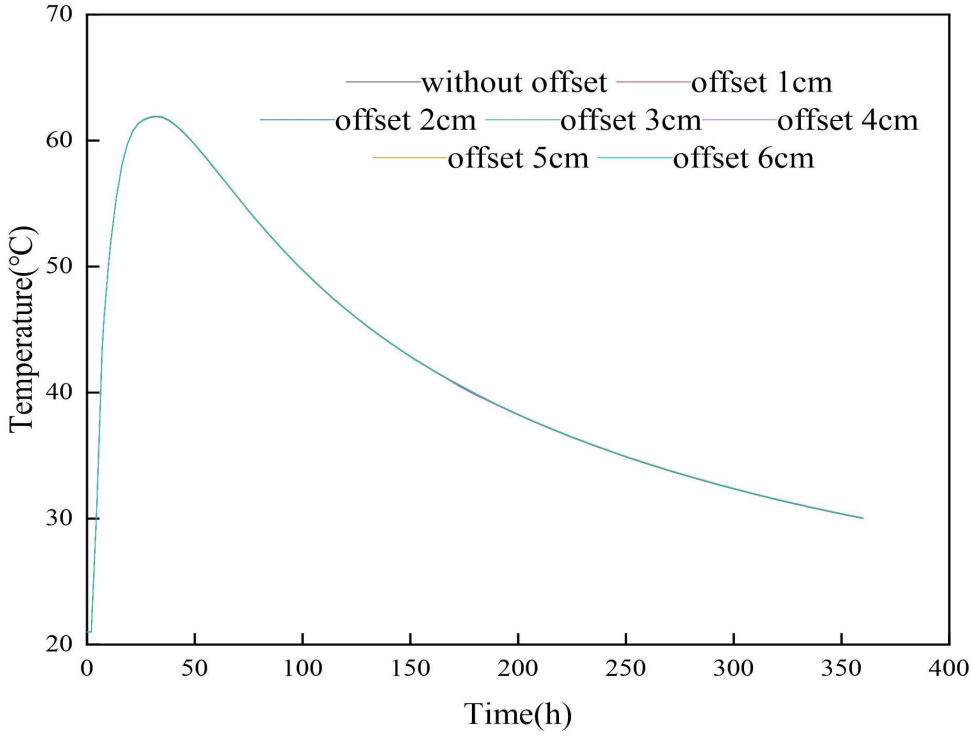

(a) Center point

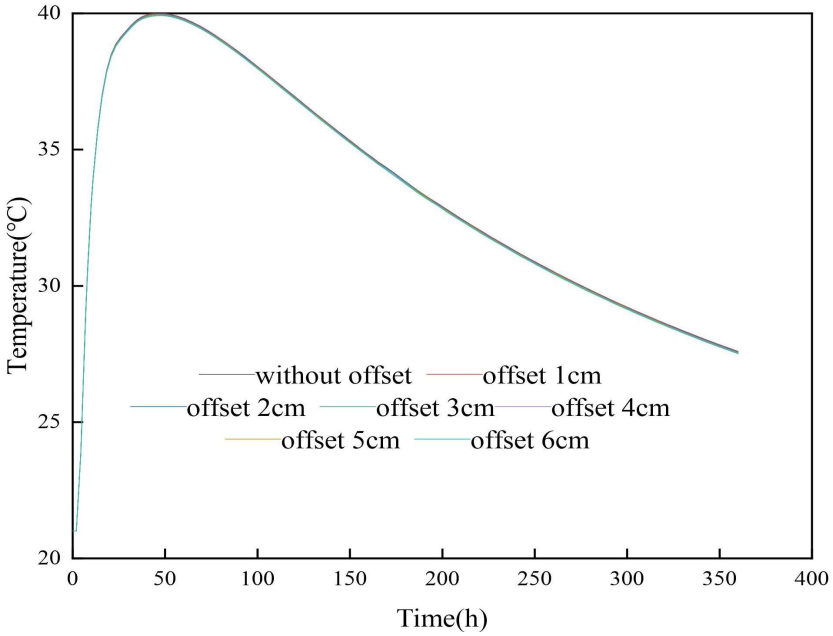

(b) Point located on the north side of the concrete edge

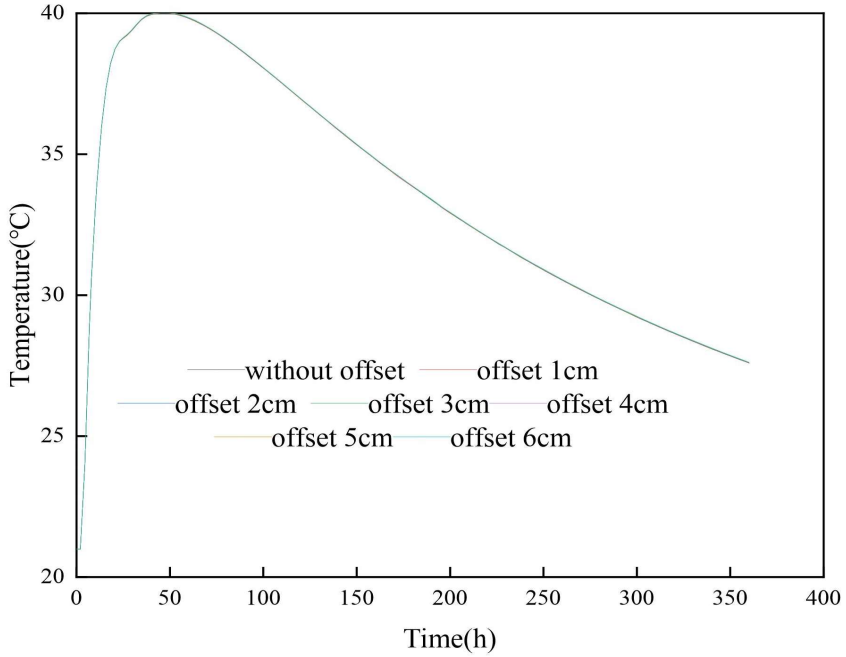

(c) Point located on the east (west) side of the concrete edge

4.3. Selection of temperature measurement points at defects

In the study of defects using the finite element method, the displacement of the reinforcement only leads to the displacement of the temperature sensor position, according to the conclusion in Section 4.2. However, this also leads to the necessity of considering the change of the temperature sensor position in the finite element inverse analysis, which is reflected mainly in the division of the mesh at the cross section. In the existing analysis of defects using the finite element method, the displacement of the defect and the position of the reinforcement are

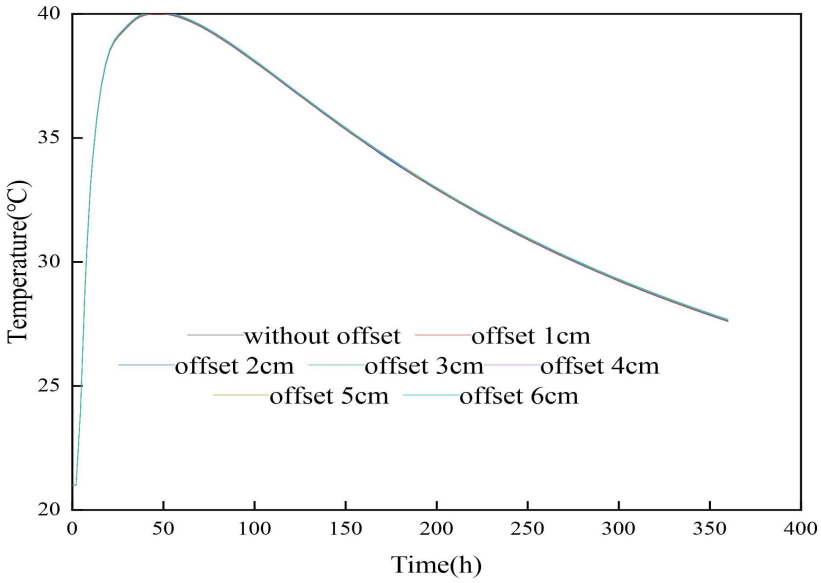

(d) Point located on the south side of the concrete edge.

Figure 9. Temperature variation curves with time at different points at 25-m cross section

considered at the same time. This also leads to too many finite element inverse analyses, so that the results of the analysis do not reflect the actual situation. Therefore, it is necessary to find new measurement points to improve the efficiency and accuracy of the finite element inverse analysis.

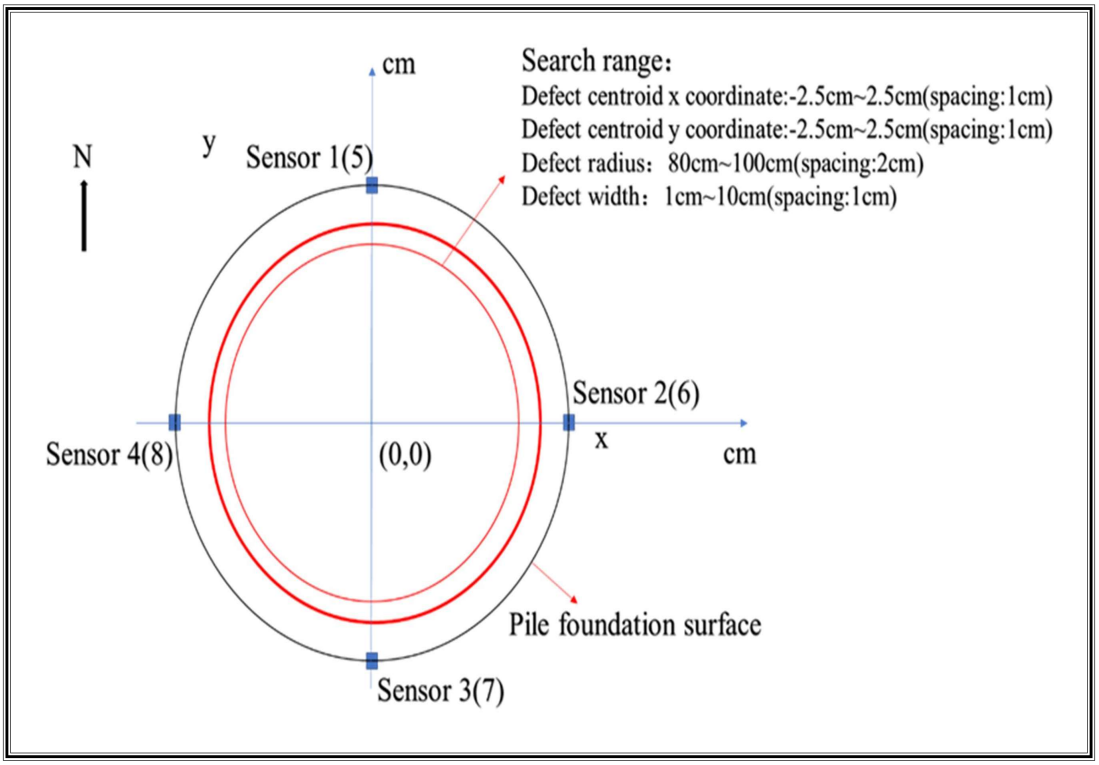

(a) Top view

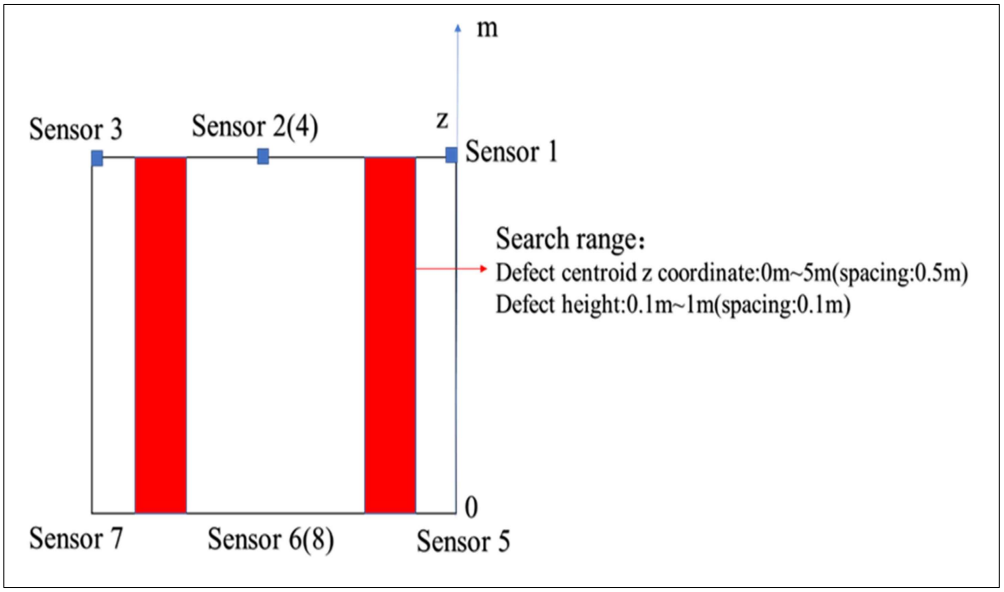

(b) Side view

Figure 10. Finite element model defect configuration

The method of inverse analysis is consistent with the method used by Sun et al. [10]. First, the possible locations of the defects can be determined based on the temperatures measured at each measurement point. Then the shape of the defect can be assumed and the search area can be delineated. Next, the defect locations and the step size of the search can be set, and the simulation can be performed step by step for the chosen step size. After each simulation, the calculated and measured temperatures of each measurement point on the concrete surface should be compared. And the "cost minimization function" should be calculated. It can replace the defect location and size corresponding to the minimum value of the cost minimization function for the final defect location and size. As shown in Figure 10, in this study the area at depths of 40-45m was analyzed, and the corresponding cross sections were located at depths of 40 and 45m. The searched grid (0.05 × 0.05 ×5 m) has 396 search points. The numerical model was used to simulate a cylindrical ring anomaly centered on 250 search points with an inner radius between 0.8 and 1 m (0.02-m step for each simulation), a width between 0.01 and 0.1m (0.01-m step for each simulation), and a height between 0.5 and 2.5m (0.5-m step for each simulation). A total of 287,496 simulations were performed.

The location and type of defects were analyzed inversely according to the steps described in section 4.3.1. The results of the analysis are pictured in Fig. 9 and show that there is a defect in the shape of a cylindrical ring at (0.5cm, 0.5cm, 4m) with an inner diameter of 98cm, a width of 9cm, and a height of 1m.

Figure 11 compares the simulated and measured results of the temperature sensor and the finite element simulation at the well wall at depths of 40 and 45m. It can be seen that the measured value of the temperature measurement point at 45m is in good agreement with the calculated value. Although the measured value of the temperature section at 40m deviates from the calculated value, the maximum difference does not exceed 3%.

There are several possible reasons for the discrepancy. First, the thermal parameters of the fully weathered conglomerate were set to a uniform value in Section 4.1.4. However, the thermal parameters of the fully weathered conglomerate at 40 m may actually differ from those at other depths. Second, the measured values of the temperature at the four measurement points at 40 m are less than the calculated values, which indicates that there may be other defects in this section that contribute to temperature reduction, such as cavities or necking.

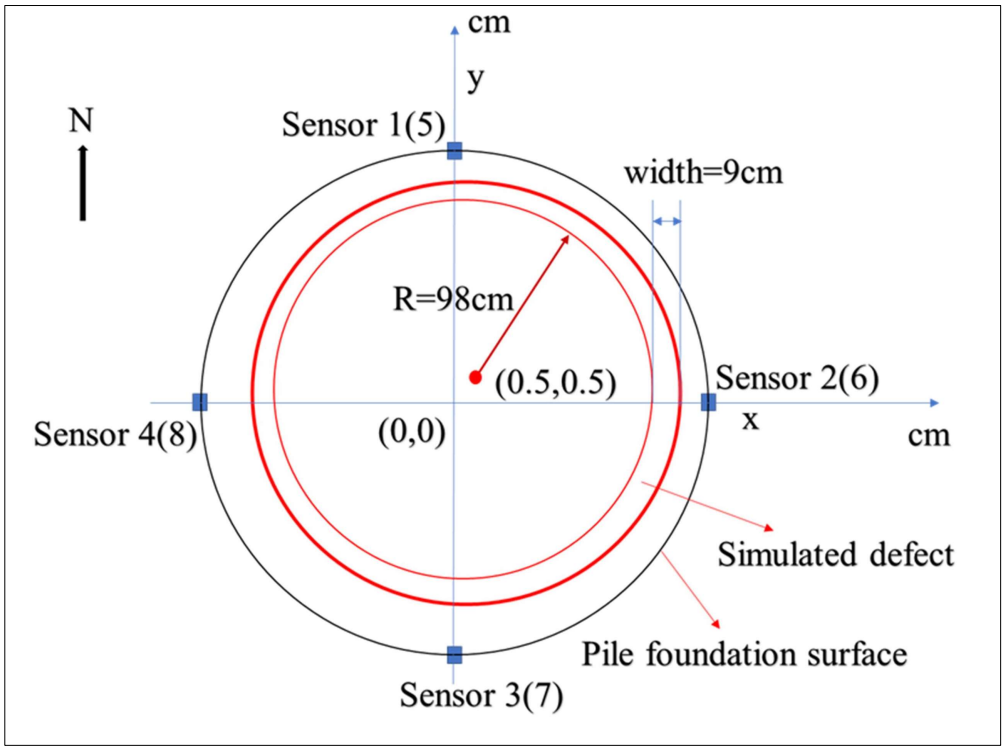

(a) Top view

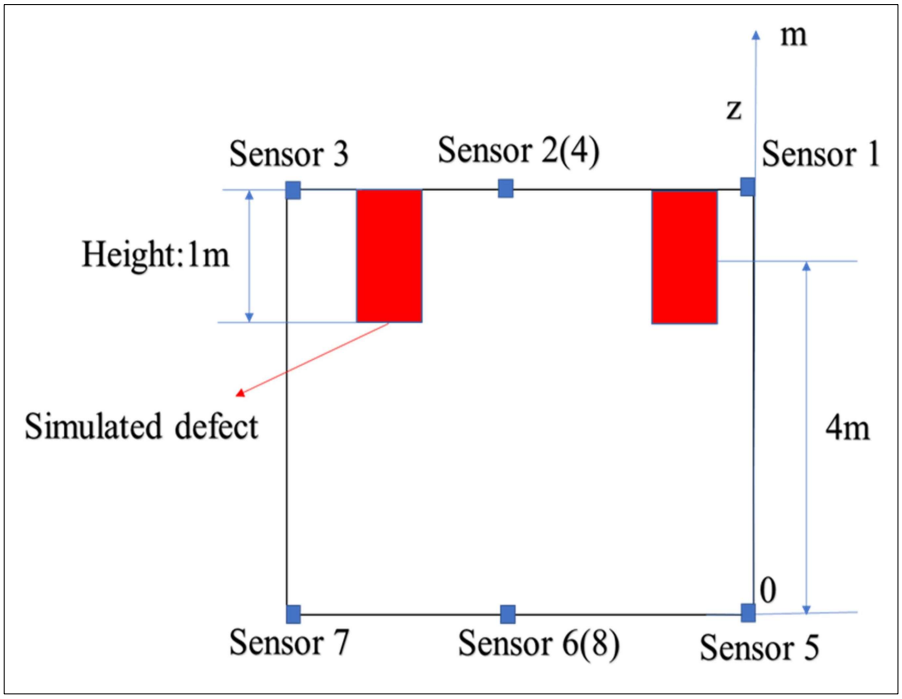

(b) Side view

Figure 11. Defect simulation results

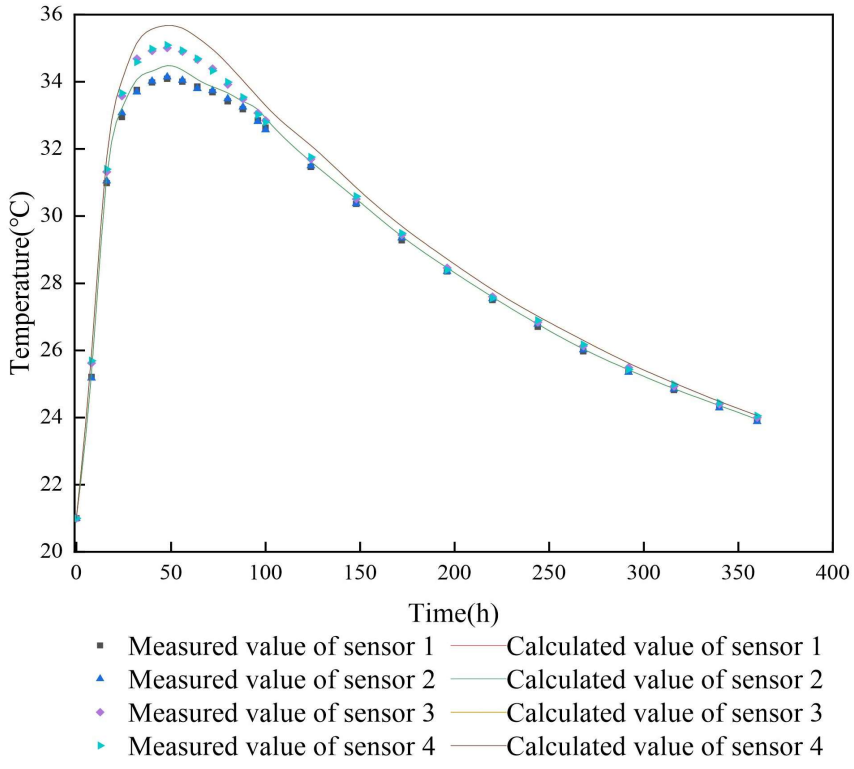

(a) At 40 m

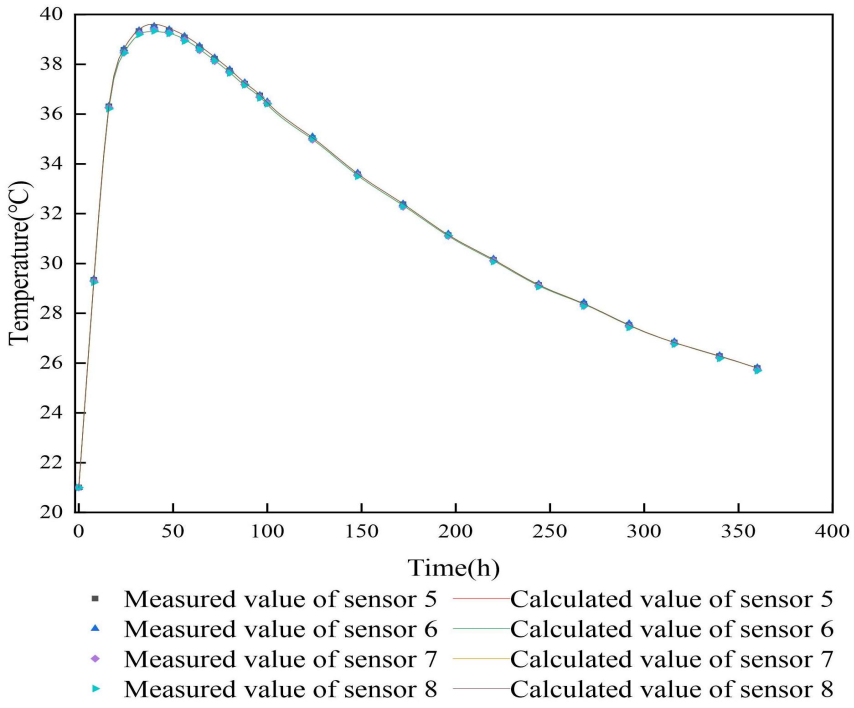

(b) At 45 m

Figure 12. Comparison of calculated and measured temperatures

5. Conclusions

The early concrete hydration heat temperature field has been used by other researchers in a thermal imaging profiler (TIP) to assess the integrity of various structures, including pile foundations, diaphragm walls, and dams. The inverse analysis of pile foundation defects using the finite element method has achieved positive results. However, the selection of temperature measurement points increases the difficulty of the inverse analysis and also reduces the accuracy of concrete defect identification due to the location of temperature measurement points. In this work, we chose to arrange the measurement points at the positions of pile foundation pit walls. The results show that the improved arrangement of temperature measurement points eliminates the need to consider the factor of reinforcement cage displacement in the existing method and further improves the accuracy of the finite element inverse analysis. The following conclusions are drawn.

(1). *The finite element simulation leads to the key conclusion that the displacement of the reinforcement cage only affects the location of the temperature measurement points and does not affect the temperature field of the concrete itself. This can not only provide a theoretical basis for the reselection of the measurement points, but also demonstrate that the displacement of the cage need not be considered directly in the finite element simulation, but only in the mesh division.*

(2). *By arranging temperature measurement points around the hole, the temperature data of the concrete surface was obtained. These measurement points were then used to perform inverse analysis of concrete defects. Compared with the existing study, the relative error of the temperature change is within 3% of its maximum value. The location and size of defects are closer to the actual location and size. In addition, the influence of the reinforcement cage displacement does not need to be considered during the inverse analysis, which further simplifies the existing method.*

(3). *Only conventional temperature sensors were used for temperature measurement in this study. And only concrete surface measurement points were selected for finite element inverse analysis. The next study can use higher-density temperature measurement equipment, and more temperature measurement points can be selected for inverse analysis to further improve the accuracy of concrete defect identification.*

Acknowledgments

We gratefully acknowledge PowerChinaRoadbridge Group CO.LTD for providingresources and facilities that made testing and research possible.

- *Disclosure statement*
- *No potential conflict of interest was reported by the author(s).*

- *Notes on contributors*
- *Mr. Zhiguo Ma is currently a senior engineer at PowerChinaRoadbridge Group CO.LTD, China.*
- *Mr. Chenjin Shi is currently a senior engineer at PowerChinaRoadbridge Group CO.LTD, China.*
- *Mr. Yuan Hou is currently a senior engineer at PowerChinaRoadbridge Group CO.LTD, China.*
- *Mr. Chao Xue is currently a senior engineer at PowerChinaRoadbridge Group CO.LTD, China.*
- *Mr. Minghao Sun is currently a graduate student at School of Civil Engineering, Southwest Jiaotong University, China. His research focuses on pile foundation defect detection and heat transfer.*
- *Mr. Yong Zeng is currently associate professor at School of Civil Engineering, Southwest Jiaotong University, China. He has Published 5 journal papers to his credit. His pedagogical*

interests include but not limited to: Railway, highway and urban rail transit line design theory and method, line BIM technology.

Declarations of interest

None

References

[1] Matsumoto, T., Kitiyodom, P., Matsui, H., Katsuzaki, Y. (2004). Monitoring of load distribution of the piles of a bridge during and after construction. *Soil Found*, 44(4), 109-117.

[2] Kister, G., Winter, D., Gebremichael, Y. M. (2007). Methodology and integrity monitoring of foundation concrete piles using Bragg grating optical fibre sensors. *Eng Struct*, 29(9), 2048–2055.

[3] Mullins, G. (2010). Thermal integrity profiling of drilled shafts. *J Deep Found Inst*, 4(2), 54–64.

[4] Liu, Y. L., Xiao, H. L., Hu, Q. Z., Ma, Q., Li, L. H. (2017). Research on Integrity Detection Method for Bored Pile Using Distributed Optical Fiber Temperature Sensing Technology. *Journal of Yangtze River Scientific Research Institute*, 34(6), 124–127.

[5] Liu, Y.L., Huang, S.L., Xiao, H.L., Chen, W.Z., Ma. Q. (2019). Research on optimization of optical fiber layout for DTS detection of bored pile integrity. *China Journal of Rock Mechanics and Engineering*, 38(S2), 3841–3848.

[6] Liu, Y.L., Ding, H., Wang, K.B., Xiao, H.L., Li, L.H. (2020). Thermal conduction characteristics of DTS when detecting the integrity of cast-in-place piles considering their environment. *Heat and Mass Transfer*, 56(5), 2185-2202.

[7] Chen, Z., Sun, Y., Liu, Y.L., H.L. Xiao., L.G. Zhang. (2020). Study on temperature field characteristics of heat source in necking cast-in-place pile based on ANSYS. *China Sciential and Technical thesis*, 15(10), 1169-1176.

[8] Chunge, M. (2014). Monitoring the integrity of bored concrete piles using distributed fibre optic sensors. MPhil thesis, *University of Cambridge*, Cambridge.

[9] Andrew, Z., Boeckmann, J., Erik, Loehr. (2019). Evaluation of Thermal Integrity Profiling and Crosshole Sonic Logging for Drilled Shafts with Concrete Defects. *Transportation Research Record*, 2673(8), 86-98.

[10] Sun, Q. C., Elshafie, M., Barker, C., Fisher, A., Schooling, J., Rui, Y. (2021). Thermal integrity testing of cast in situ piles: An alternative interpretation approach. *Structural Health Monitoring*, 20(5), 2493-2512.

[11] Sun, Qianchen., Elshafie, M, Z.E.B., Barker, C., Fisher, A., Schooling, J., Rui, Y. (2022). Integrity monitoring of cast in-situ piles using thermal approach: A field case study. *Engineering Structures*, 272, 1-16.

[12] Mullins, G., Johnson, KR. (2016). Optimizing the use of the thermal integrity system for evaluating auger-cast piles. *Final report, FDOT-BDV35-977-09*, Tallahassee, FL: Department of Transportation.

[13]*ASTM D7949-14*. Standard Test Methods for Thermal Integrity Profiling of Concrete Deep Foundations.

[14] Zhu, Bofang. (2003). Temperature Stress and Temperature Control of Mass Concrete. *Beijing: China Electric Power Press*.

[15] Zhang, J. R., Liu, Z. Q. (2006). A study on the convective heat transfer coefficient of concrete in wind tunnel experiment. *China Civil Engineering Journal*, 39(9), 39-42+61.

[16] Rui, Y., Kechavarzi, C.-O., Leary, F., Barker, C., Nicholson, D., Soga, K. (2017). Integrity testing of pile cover using distributed fiber optic sensing. *Sensors*, 17(12).

[17] De, Schutter, G., Taerwe, L. (1995) General hydration model for Portland cement and blast furnace slag cement. *Cement Concrete Research*, 25(3), 593–604.

[18] Zhu, Bofang. (2009). New progress of concrete dam theory and technology. *Beijing: China Water Resources and Hydropower Publishing House*, 2009.

[19] Schindler, K., Folliard, J. (2005). Heat of Hydration Models for Cementitious Materials. *ACI Materials Journal*, 102(1), 24-33.

[20] Xue, S. D., Kang, G. B., Li, X. Y., Gen, Y., Li, J. G., Song, Y. J. (2020). Hydration Temperature Field of Large-size Concrete Member During Hardened Period. *Journal of Beijing University of Technology*, 46(2), 147-153.

[21] Ma, Chao. (2020). Temperature field of mass concrete based on BP neural network positive and negative analysis research. MPhil thesis, *Changsha University of Science & Technology*, Changsha.